

NUMERICAL STUDY OF UNSTEADY FLOWFIELD AROUND HIGH SPEED TRAINS PASSING BY EACH OTHER

First author : Jaeho Hwang*

Affiliation: Ph.D candidate, Dept. of Aerospace Engineering, Seoul National University
Address: BD136-317, Seoul National University, Seoul 151-742, Republic of Korea
phone: +82-2-880-8051
fax: +82-2-889-6205
e-mail: aerj@bigfoot.com

Second author : Tae-Seok Yoon

Affiliation: Ph.D candidate, Dept. of Aerospace Engineering, Seoul National University
Address: BD136-318, Seoul National University, Seoul 151-742, Republic of Korea
phone: +82-2-880-8051
fax: +82-2-889-6205
e-mail: TSYOON@snu.ac.kr

Third author : Dong-ho Lee

Affiliation: Professor, School of Mechanical and Aerospace Engineering,
Seoul National University
Address: BD301-1302, Seoul National University, Seoul 151-742, Republic of Korea
phone: +82-2-880-7386
fax: +82-2-887-2662
e-mail: dhlee@gong.sun.ac.kr

Fourth author :Soo-gab Lee

Affiliation: Professor, School of Mechanical and Aerospace Engineering,
Seoul National University
Address: BD301-1418, Seoul National University, Seoul 151-742, Republic of Korea
phone: +82-2-880-7384
fax: +82-2-887-2662
e-mail: solee@plaza.sun.ac.kr

Keywords

High speed trains, Moving grid system, Train/tunnel interaction, Train/train interaction, Unsteady aerodynamic loads, Domain decomposition technique, Parametric study

Abstract

In order to study unsteady flowfield around high speed trains passing by each other, a three-dimensional inviscid numerical method based on three types of domain decomposition techniques is developed. Roe's FDS scheme is used for the space discretization, and LU-SGS method is adopted for the time integration. After validation of the code to a single track train/tunnel interaction problems with three dimensional tunnel configuration, the numerical simulations of the trains passing by on the double-track are for the 5 different cases using 3 basic parameters; e.g. nose shape, existence of tunnel, and train length. After the parametric study, variational parametric studies are carried out to understand the effects of the velocity of the train, the gap between the train and the blockage ratio. Firstly, train/tunnel interaction problems for double track railway system are investigated and aerodynamics loads histories during the crossing events -train/train interaction problem - are presented and discussed.

I. Introduction

The success obtained by Japanese National Railways' long-distance Shin Kansen 210km/h services since 1964 as well as SNCF's(Societe Nationale des Chemins de fer Francais) conventional special trains and British Railways' high-speed train(HST) 200km/h services since the late 1960s or the mid 1970s, respectively, has clearly proved that high speed is one of the main assets of railways in highly industrialized countries, in which they have been continuously losing ground to individual road traffic in the last four decades. For the rapidly increased speed of a high speed train, aerodynamics is of paramount importance in the development of very high speed trains, as it is one of the main factors influencing the dimensioning of the traction motors and the suspension system, operating costs, safety, comfort and environment¹.

When a train enters a tunnel at high speed, a compression wave is generated ahead of the train, and propagates along the tunnel. At the tunnel exit, the compression wave is reflected back into the tunnel forming an expansion wave. Such waves create unfavorable aural effects, causing discomfort on passengers during tunnel passing. A resident near-by tunnel exit portals, on the other hand, can suffer from the noise and vibrations (phenomena designated as sonic boom) caused by the transmission of an impulsive pressure wave called a micro-pressure wave.

When two trains cross each other, 3-dimensional unsteady impulsive aerodynamic loads may induce the instability of the trains, leading to unfavorable snake-like motions by push-pull like side force. And much larger pressure fluctuation over the trains would be expected during the crossing event, but the details of the flow properties are not well understood as yet.(see figure 1) Thus, to enhance the passenger comfort and the stability of the train, with the extension of operational speeds to 350km/h or higher, better understandings of the unsteady flow phenomena induced by the relative motions between train and tunnel(train/tunnel interaction) and between two trains(train/train interaction) are required.

In the current study, 3-dimensional compressible, inviscid code is developed to analyze the flow

field around the high speed trains in relative motion at the open space and in the tunnel. Since the viscous effects on the wave characteristics are negligibly small as is shown by Maeda², and since we do focus on the global flow characteristics, not on the details of the flow field around train, e.g. underflows, wake regions at the tail, and flows around skirt, etc., the inviscid assumption would be sufficient for the purpose. A higher order Roe's upwind scheme³ with MUSCL and van Albada limiter function⁴ is employed to simulate properly the whole pressure wave phenomena - generation at the entrance, propagation through the tunnel, radiation and reflection at the end of the tunnel and interaction again with the trains. A smart moving grid system based on domain decomposition techniques is developed and applied to study the unsteady flow fields induced by the restricted linear motion of a train on a rail. Due to the prescribed motion of a train on the rail, the grid system could be tuned up for this case without considering the generality and consequently requires less computational resources, as suggested by Hwang and Lee⁵.

The developed code firstly is applied to a single track train/tunnel interaction problem with 3 dimensional tunnel configuration and compared with experimental results. The results show good agreement with experimental values.

The numerical simulations of the trains passing by at the double-track at 350 km/h are carried out for 2 nose shapes to study the effect of the nose shape. The configuration of the trains/tunnel model is based on the configuration of the KHST (Korean High Speed Train) under development. The difference of the flow phenomena due to the crossing region is studied for the trains passing by at the open space and inside the tunnel. And, the number of cars of a train is changed to examine the length effect and to study side force variation - push-pull like side force - on each car. Finally, the effects of the velocity of the train, the gap between the train and the blockage ratio are studied through computations. Thus, a parametric study on the flow field around trains passing by each other is performed to understand basic nature of the crossing event using the nose shape, the crossing location, the train length, the speed of train, the gap and

the blockage ratio as parameters.

This paper is organized as follows. In section II, numerical procedure adopted in the current study is introduced including the grid system. In chapter III, the computed results on single track train/tunnel interaction problem are given and in chapter IV, double track train/train interaction problems are defined and the computed results are presented and discussed. Finally, concluding remarks are drawn.

II Numerical Procedures

Euler equations with a smart moving grid system are used to analyze the flow field originating from the aerodynamic interaction of train and tunnel and of train and train.

II.1 Numerical algorithm

The unsteady, compressible and three-dimensional Euler equations are solved to analyze the flow field around the high-speed train. The system of equations consists of a local time derivative term and three convective flux vectors. In physical coordinates, the governing equation is:

$$\frac{\partial Q}{\partial t} + \frac{\partial E}{\partial x} + \frac{\partial F}{\partial y} + \frac{\partial G}{\partial z} = 0 \quad (1)$$

where

$$Q = \begin{pmatrix} \rho \\ \rho u \\ \rho v \\ \rho w \\ \rho e \end{pmatrix} \quad E = \begin{pmatrix} \rho u \\ \rho u^2 + p \\ \rho uv \\ \rho uw \\ (\rho e + p)u \end{pmatrix} \quad F = \begin{pmatrix} \rho v \\ \rho uv \\ \rho v^2 + p \\ \rho vw \\ (\rho e + p)v \end{pmatrix} \quad G = \begin{pmatrix} \rho w \\ \rho uw \\ \rho vw \\ \rho w^2 + p \\ (\rho e + p)w \end{pmatrix}$$

The equation of state is as follows.

$$e = \frac{1}{\rho(\gamma - 1)} p + \frac{1}{2} (u^2 + v^2 + w^2) \quad (2)$$

where γ is the ratio of specific heats.

Roe's finite volume flux difference splitting technique based upon the solution of the Riemann problem³ is used for spatial discretization and MUSCL (Monotone Upstream-centered Scheme Conservation Laws) with van Albada flux limiter⁴ is used to achieve the third order of spatial accuracy. Calculations of unsteady flow-field around moving body require a time accurate numerical integration. In the present study, Yoon's LU-SGS scheme⁶, an implicit scheme, is chosen for efficient time marching due to the huge demand on computer power for such three-dimensional computation. More elaborative introduction to the numerical method presented in this chapter can be found in reference⁷.

II.2 Grid systems

The grid system for the computation of the three dimensional train/tunnel interaction and train/train interaction is characterized by a moving body confined to linear motions on the rail, relative motions between solid bodies, ground proximity and relatively very long tunnel through which trains go. Thus, it may take huge computational resources to use conventional grid systems such as Chimera grid^{8,9} and unstructured grid¹⁰, both in time and storage device.

To accommodate the relative motion, Fujii and Ogawa^{11,12,13} used FSA(Fortified Solution Algorithm)¹⁴, and they successfully computed tunnel entry problem and crossing problem. Fujii's approach on the current problem is similar to the Chimera procedure⁸ composed of hole construction and linear interpolation at boundaries, thus a strict criteria on boundaries such as moderate cell volume ratio between giving cell and target cell is necessary to get stable solution. If the region to be swept by the train is large, there should be gigantic number of grid points along the region in order to satisfy the proper interpolation criterion through the whole 3-dimensional computational domain. Fujii and Ogawa used intermediate zone to overcome this requirement, but it makes the computations inefficient because of the intermediate zone which requires more linear interpolations.

As an alternative, Mestreau¹⁰ used the unstructured grid system with automatic re-meshing and Holmes¹⁵ applies moving boundary condition to the tunnel wall, using a flow solver based on GLS finite element formulation. These grid systems were applied to limited cases, e.g. tunnel entry problem, and they are not suitable for parametric studies using several parameters because of costly re-meshing and sophisticated assumptions on the boundary condition.

Hwang and Lee⁵ suggested that the grid system could be tuned up for computational efficiency avoiding costly unsteady re-meshing and sophisticated assumptions on the grid system by careful choice of domain decomposition techniques adapting the linear motion on a rail.

In the current study, 3 types of domain decomposition techniques, multi-block grid, patched grid, and overlapping grid are applied regarding computational efficiency and extensibility. Figure 2 shows the schematic diagram of the grid system and the zonal interface for the tunnel entry problem. The extensions of the grid system to tunnel outgoing problems and train/train crossing problems are straightforward just by adding an extra computational domain at the exit region(see figure 4) and by imposing line symmetric boundary condition(see figure 8).

Zone 1 is a moving zone around a train, and zone 2 is a background zone where zone 1 is overlapped. Consequently a simplified Chimera hole construction and linear interpolation routines between zone 1 and zone 2 are needed only at the fore and aft part of the zone 1. These interpolations at the fore and aft part of the zone 1 are reduced to 1-dimensional.

Compared with the 3-dimensional Chimera procedures, the current method is much more efficient because it uses much fewer fringe cells and does not use additional iterations to find interpolation coefficients. In addition, if the cell volume ratio at the boundary is order of 1, the interpolation process is thought to be conservative because the linear interpolation is performed by the cell volume ratio. Considering the mild variation of the flow variables except the vicinity of the train and 1-dimensional wave phenomena in the tunnel, the linear interpolation can be used with great reliability and without adopting a tedious 3-dimensional conservative treatment.

As an intermediate zone, zone 3 shares a sliding surface with zone 1, and conservative patching

algorithm is applied at the surface. By using this intermediate zone, code extension to the crossing case can be realized in a simple manner. Zone 4 is a tunnel entrance zone. For the computation of unsteady flow field around a train going into/out of a tunnel, simply adding the zone 5 at the other ends of tunnel is sufficient for the whole flow field as shown in figure 4. Figure 8 shows a schematic of grid system for a computation of the crossing case. By generating the grid system on the one half of the double track, and by applying a line symmetric boundary condition on the inner symmetric surface of the intermediate zone, simulations of the crossing event on the double track can be realized without other changes of the grid topology and the solver.

III. Single Track Train/Tunnel Interaction

III. 1 Description of the case

For the validation of the current code, experimental investigations were carried out in the Train Tunnel Test Facility (T3F) at National Aerospace Laboratory (NLR) in Netherlands under a contract with Seoul National University.

In the experiment, cross-sectional areas of train and tunnel model with its blockage ratio (ratio of cross-sectional area) are 314.2 mm^2 , 3880 mm^2 and 8.1% respectively. The shape of the model train is given in figure 3.

The pressure fluctuations in the tunnel were recorded at 4.3% of the total length of the tunnel from the inlet by using pressure transducers (Endevco, type 8510B-2) of 13.8 kPa dynamic range and 70 kHz resonance frequency. Two different tunnel entrances were used in the test to investigate the effect of the configuration of the tunnel: a 45-degree slanted and a non-slanted entry. Detailed description about the experimental setup and results can be found in reference¹⁶.

Computations are performed about 300km/h, 350km/h, 380km/h with and without 45 degree slanted entry. For the computations, 5 block grid system is used as illustrated in figure 4, for

which the total number of grid points is 421,615. In the computations, the constant time step of $\Delta t = 0.01/\text{iteration}$ is used, and impulsive starting initial condition is used. Here, the length scale is normalized by the width of the tunnel D .

III. 2 Computational results

The propagation of compression wave along the tunnel is numerically simulated. In figure 5, it is observed that the compression wave is generated from the head of the train entering the tunnel and propagates toward the exit of the tunnel faster than the train itself at about the speed of sound.

To validate the prediction in the present study, entry compression wave at $x/L = 4.3\%$ is compared with the experimental result for 300km/h in figure 6. Because our approach uses Euler equations, the compression wave front is used for the comparison to eliminate the Reynolds number dependent displacement effect. Time is set to 0 sec when the train is located at $x = 9D$ from the entry. An accurate prediction of gradient and amplitude of the compression wave is very important in the prediction of micro-pressure wave at the tunnel exit because the strength of micro-pressure wave is proportional to the gradient of the compression wave². In the figure, computational result matches well with the experimental result both in the amplitude and the maximum gradient of the compression wave.

The characteristic of the compression wave is determined not only by the nose shape of the train but also by the configuration of the tunnel entrance. One of the countermeasures to reduce the gradient of the incident compression wave and the micro-pressure wave is the slanted portal. Figure 7 shows the effect of the slanted entry with 45-degree slant and non-slanted entry at a speed of 350 km/h. In prediction, the slanted entry was treated as a wall boundary condition using the same grid system. The effect of slanted entry can be thought to prevent the abrupt change of cross sectional area. Thus, the rising time may increase and accordingly the maximum pressure gradient may reduce. The pressure gradient of the compression wave is relatively mild

compared with the non-slanted entry as shown in figure 7.

IV. Double Track Train/Train Interaction

IV. 1 Description of the cases of crossing

Due to the difficulties in studying on the crossing event of the high speed trains, only a few and limited numerical studies^{13,17} and experimental research¹⁸ have been reported. Shimbo¹⁸ measured the pressure data at the limited points over real train surface during the crossing event and reported asymmetric pressure distributions. Fujii¹³ revealed basic nature of the crossing event by three dimensional simulation using FSA(Fortified Solution Algorithm) and Kikuchi¹⁷ suggested that unsteady boundary element method can be used to compute unsteady aerodynamic forces during relative motions between solid bodies.

Basic Parameters

In the present study, an efficient solution strategy about the crossing problem is developed to study the unsteady aerodynamic forces associated to the crossing events. Three basic parameters for the crossing problem - the nose shape(long and short frontal shapes), the location(at the open space and in the tunnel) and the length of the train(train of 2 cars and 3 cars) are adopted for the current study. Table 1 shows the definition of the adopted 5 cases with their referring name. In the computation, the velocity of the train is set to 350km/h for the cases listed in the table.

Table. 1 Definition of the cases of crossing

Case	Shape of train	Crossing location	Train length
LFCT	Long frontal shape (15m long)	In the tunnel	40m (2 cars)
SFCT	Short frontal shape (6.64m long)	In the tunnel	40m (2 cars)
LFCO	Long frontal shape (15m long)	At the open space	40m (2 cars)
SFCO	Short frontal shape (6.64m long)	At the open space	40m (2 cars)
SFCO3	Short frontal shape (15m long)	At the open space	60m (3 cars)

The shapes of the train and the tunnel are given by KHST railway system, and they are

simplified so that complexity in grid generation could be avoided. Because we concentrate on the global flow physics, e.g. force coefficients and pressure distribution along the tunnel, the shape of train is generated just to satisfy the frontal view(cross-section), the plan view, the side view and the area distribution along the nose.

Table. 2 Number of grid points and initial distances used for the crossing cases

Case	No. of grid points	Initial distance between the trains
LFCT	341,941	48.60 D(about 457m)
SFCT	488,061	66.25 D(about 623m)
LFCO	235,471	21.14 D(about 199m)
SFCO	302,051	21.14 D(about 199m)
SFCO3	316,111	21.14 D(about 199m)

The width, height and cross-sectional area of the train are 2.80m, 3.50m, and 9.00m² each. And the cross-sectional area of the tunnel is 118m². The length of the train is set to 40m, approximately twice the length of the power car except the case SFCO3 of 60m representing 3 cars. Table 2 draws the number of grid points used for each case and initial position between the trains. In order to reduce the computational time, the initial distance of the case LFCT is set to 48.60D. The height of the tunnel D is chosen as a reference length. In the computations, the global time step, $\Delta t = 0.01/\text{iteration}$ is used for all cases after the time step sensitivity study on the load histories. It takes 3.8×10^{-5} sec per grid point for 1 iteration at 450MHz DigitalTM AlphaTM CPU and the interpolation time between the domains is less than 1% of the total time per one iteration. Figure 8 shows the frontal view of the grid system used for the case SFCT.

Variational Parametric Study

In addition to the selected five cases using the 3 basic parameters - the nose length, the crossing location and the train length, 3 more variational parameters- the velocity of the train, the gap between the trains and the blockage ratio are chosen for that parametric study. In order to investigate the effect of the velocity on the crossing event, 10 cases are computed as shown in

Table 3.

Table. 3 Computed cases for the investigation of the effect of the velocity

Case	250km/h	300km/h	350km/h	400km/h
LFCO	√	√	√	√
SFCO		√	√	√
LFCT	√	√	√	

The effect of the change of the gap between the crossing trains is examined about the gaps as 1.6m, 1.9m, 2.2m, 2.5m and 2.8m. 2.2m gap is the reference value which is used for KHST railway system. The gap is adjusted just by repositioning the location of the train in the grid generation processes. For this parametric study, the case LFCT and the case LFCO are chosen as the reference configurations, thus 10 cases are solved.

For the study of the effect of the blockage ratio change, 4 cases are made by multiplying the characteristic length D of the tunnel by 0.8, 0.9, 1.0, 1.1. The case LFCT is taken as reference configuration. Thus, the blockage ratios are set to 0.063, 0.076(reference value), 0.094 and 0.119 respectively.

IV. 2 Computational results and discussions

Train/Tunnel Interaction

Because a tunnel is one of the main elements in the railway system, train/tunnel interaction due to the relative motion between trains and tunnel has been a subject studied by various researchers^{2,10-13,15,17-19}. They have used various techniques such as 1-dimensional characteristic method, CFD using 2-dimensional Euler equations, CFD using 3-dimensional Euler equations, scaled model experiment and full scale experiment.

However, their researches have not covered the whole phenomena - train/tunnel interaction and train/train interaction appropriately. In the current study, train/tunnel interaction as well as train/train interaction is studied through 3-dimensional unsteady computations.

The spatial distributions of pressure along the tunnel wall are shown in figure 9 and 10 for the case SFCT. The positions of pressure probes for the curves are given in figure 8, each named as 'p lower', 'p inner', 'p upper', and 'p outer'. The pressure is shown in real dimension, 'Pa' for those figures.

As the trains are entering the tunnel, compression waves are generated and propagated into the tunnel as shown in the figure 9. The strength of compression waves are about 934 Pa which is smaller than a value(1042 Pa) calculated by empirical formula². The formula is deduced under the assumption of 'isentropic flow', 'small amplitude', 'the depth of the compression wave front is small' and 'speed of the compression wave is constant at the front'. Thus, the values from the 3-dimensional computation and from the formula might be different each other owing to the 3-dimensional effect like the asymmetric position of the train.

In figure 10, it is shown that reflected pressure waves at the open ends of the tunnel are propagating to the opposite direction with negative pressure and they sweep the crossing event at the center of the tunnel. By the zoomed views of the crossing event in the figure, it is expected that the train may undergo complex and severe aerodynamic load conditions during the crossing event.

The spatial distributions of pressure along the tunnel wall are shown in figure 11 and 12 for the case LFCT. Sequentially, they are showing 'generation of the compression waves', 'propagation and linear addition of the pressure waves' and 'the crossing event'. Due to the elongated nose, the spatial gradients of the compression waves are smoothed and due to the mild flow gradient around the noses, the negative pressure region around the trains does not seem to be stiff even during the crossing event.

It can also be pointed out from the figures that except the vicinity of the trains the flow field in a tunnel is nearly 1-dimensional.

Train/Train Interaction

Aerodynamic load histories are examined in order to understand basic nature of the crossing event using the nose shape, the crossing location and the train length as parameters. The loads are non-dimensionalized to the aerodynamic load coefficients as are depicted in the figure 1, C_D , C_S , C_L by using the dynamic pressure and the reference cross sectional area of the train. The time for load histories is set to zero when the trains start crossing, and accordingly $t = 15.32$ when the trains end crossing. At $t = 7.66$, the two trains are located exactly side by side. And the duration of the crossing event is increased by factor 1.5 for the case SFCO3 according to the elongated length of the train by the same factor.

Figure 13 show the aerodynamic load histories of the case SFCO and SFCO3 respectively. The variations of loads with respect to time show similar pattern. Among the aerodynamic forces, unsteady side force is most significant and influential to the stability of the crossing trains. When the two trains are advancing to each other, they start pushing away each other due to the high pressure region around the noses. So, the C_S curves have maximum positive peak around 1 - 2 seconds after the two noses meet depending on the nose length. And, following the progressive overlapping of two trains, low pressure region at the inner side of the nose part induces the attracting forces, and the attracting force reaches the maximum value when the 2 trains are located exactly side by side. And, as they start parting away from the full overlapping position, the side force changes the sign from attracting to pushing again.

Aerodynamic drag histories during the crossing show similar patterns for all cases, decreasing and increasing, and they resemble point-symmetric curves at the point about $t = 7.66$ for the cases of 2 cars. When the fore nose is located at the side of the opposite train, the stagnation pressure of the nose is weakened at the side and consequently drag force is decreased. And, when the aft nose is positioned at the side of the opposite train, drag force is increased because of the weakened base pressure.

Lift curves, which is not so important for the heavy ground vehicles, show negligible variations

with small overall values.

In figure 14, comparisons of side force coefficient(C_S) and drag coefficient(C_D) for the cases of 2 cars are given. By comparing the figures, it can be concluded that the time derivatives of the force coefficients are mainly affected by the nose shape of the train. This could be explained by the differences of the spatial distributions of flow properties that sweep the opposite train. And, it can be carefully argued from figure 14-a) that the strength of the side force mainly depends upon the nose shape. Because the difference of pressure distribution between inner and outer side of the train surface during the crossing event is chiefly affected by the pressure field around the nose of the opposite train, the side force mainly depends upon the nose shape of train, not on the existence of tunnel.

From figure 14-b), it is noticed that the strength of the drag variation is mainly affected by the location where the crossing event occurs. Because the stagnation pressures of the two nose shapes are almost the same, and because the 1-dimensionality of flow in the tunnel is valid even during the crossing event, the C_D curves' trend mainly depends on the location where the crossing events occur, not on the nose shape of the train.

In general, a train consists of many cars connected one by one by articulated connectors which permits yawing motions to each separated car. So the information about the side force distribution on the each separated car is indispensable data to design and analyze the bogie system of a train. Aerodynamic load histories can be taken for each car, if we perform the force integration over the separated parts, not over the whole surface (see figure 15). For the side forces, the curve for each car shows similar pattern and slightly different temporal distribution, which may result in severe snake-like motions of the train during the crossing. The aerodynamic side force histories on each car have two dramatic changing parts - push-pull part when the fore nose of the opposite car sweeps the car, and pull-push part when the aft nose of the opposite car sweeps it away. The time interval between the push-peak and the pull-peak is proportional to the nose length. The shorter the nose is, the narrower the interval will be. And the time interval

between the two push-pull parts is proportional to the train length. The force on the fore car changes from +20,000N to -10,000N in 0.1 second at the beginning of the crossing event, which can be treated as a great impulse on the nose.

We can expect that all the mid-cars of the real train might undergo the same aerodynamic load of the mid-car of the case SFCO3. In order to extend the current results to a multi-car train without re-computation using enormous number of grid points, some time scale should be defined as shown in figure 16. T_1 denotes the duration of the aerodynamic load variation, which is proportional to the train length at the given speed of a train. T_2 denotes the duration of push-pull part and pull-push part, which is proportional to the length of the nose and so to the length of one car approximately. For mid cars of a multi-car train, the push-pull part (segment A-B) induced by the fore nose of the opposite train and the pull-push part(segment C-D) would be repeated and the segment E would be elongated proportional to T_1 . So, simply by shifting the curves fore and aft about T_2 - exactly $(\text{the length of a car, } 20\text{m})/(\text{the speed of train, } 97.6\text{m/s})/2$, the side force histories of the fore and the aft cars to a given mid car can be guessed as shown in figure 16. In the figure, it is shown that mid cars which are 20m long and running at 350km/h might undergo the opposite directional side forces for two adjacent cars. (points A, B, C, D), which could induce a severe snake-like motion.

Top views of pressure field of the ground and the train for the case LFCT and LFCO are drawn in figure 17 and figure 18. The strength of pressure variation of the case LFCT(inside a tunnel) is much higher than that of the case LFCO(open space). However, it is demonstrated that nearly 1-dimensional pressure distributions in the tunnel are valid as is pointed earlier as the reason for the drag dependence on the locations.

Effect of the velocity

In order to investigate the effect of the velocity on the crossing event, 10 cases are computed as listed in table 3. Figure 19-a) shows C_s histories with velocity changes for the case LFCO at V_T

= 250km/h, 300km/h, 350km/h and 400km/h respectively. As shown in the figure, the variations of the side force coefficients are negligible with the change of the speed. Though the nose shape is more stiff, C_S is not affected by the velocity of the train as shown in the figure 19-b) for the case of SFCO. When the trains are crossing in the tunnel, C_S does not seem to be affected by the velocity of the train as shown in the figure 19-c) which draws C_S histories with velocity changes for the case LFCT at $V_T = 300\text{km/h}$, 350km/h and 400km/h respectively. From the results, it can be concluded that the side force is proportional to the square of the train velocity (V_T) regardless of the location and the nose shape.

Effect of the gap

As is described in section IV.1, 10 cases are computed in order to investigate the effect of the velocity on the crossing event. The adopted gaps are 1.6m, 1.9m, 2.2m, 2.5m and 2.8m. The 2.2m gap is the reference value which is used at KHST railway system.

In the current study, it is argued that the presence of the tunnel when the trains are crossing is not main factor affecting side force variation. However, when it comes to quantitative research, the presence of tunnel might be considerably influential. Thus, the case LFCO and the case LFCT are used for the study.

In figure 20-a), C_S histories with gap changes for the case LFCO are shown, and from the figure it can be argued that there exists a explicit dependency between the side force and the gap. Figure 20-b) which draws C_S histories with gap changes for the case LFCT shows similar patterns compared to those of the case LFCO. Push peaks are increasing and pull peaks are decreasing as the gap is getting smaller. Thus, the maximum change will be increased as the gap decreases. The peak values of the case LFCT seems to be lager than those of the case LFCO in the figures. Thus, it can be easily mis-concluded that the existence of the tunnel might magnify the 'train/train interaction'.

In order to investigate this trend quantitatively, three output parameters are defined as shown in

the figure 21. $(C_S)_{\max}$ and $(C_S)_{\min}$ are the push peak and the pull peak respectively, and the difference $(\Delta C_S)_1$ is $[(C_S)_{\max} - (C_S)_{\min}]$.

Comparison of the defined output parameters along gap changes between the case LFCT and LFCO is shown in figure 22. The differences of $(C_S)_{\max}$ between the two cases do not vary with the gap changes, and so do the differences of $(C_S)_{\min}$. When the trains are crossing in the tunnel(case LFCT), the two peak values are increased together, so the $(\Delta C_S)_1$ is not changed much when compared with the changes of the peak values of the case LFCO. It is because of the steady suction effect to the nearer wall due to the eccentric position of the train as is shown in the figure 20-b). Judging from those two fact, 1) $(\Delta C_S)_1$ is not changed much and 2) the differences of the peak values are mainly affected by the steady side force, it can be argued that the existence of the tunnel do not affect the side force variations during the crossing.

Effect of the blockage ratio

In order to investigate the effect of the change of the blockage ratio on the side force, four cases are computed and compared. The adopted blockage ratios are 0.063, 0.076, 0.094 and 0.119 about the LFCT configuration and the result is depicted in figure 23. As shown in the figure 23-a), C_S curves are shifted as the B/R increases. Thus, $(C_S)_{\max}$ and $(C_S)_{\min}$ are increased as the B/R increases. This is due to the steady pushing side force as is pointed just before. However, $(\Delta C_S)_1$ remains constant though the B/R changes as shown in the figure 23-b).

Thus, it can be concluded that the B/R changes do not affect the side force variation if the maximum change is concerned, though stronger compression waves and negative pressure around train might cause severe pressure conditions.

V. Concluding Remarks

In order to study unsteady flow-field around high speed trains passing by each other, a three-

dimensional inviscid numerical method based on three types of domain decomposition techniques is developed and applied. After the validation of the current code to a single track train/tunnel interaction problems, the numerical simulations of the trains passing by on the double-track are conducted for the 5 different cases using the 3 basic parameters; e.g. different nose shape, existence of tunnel, and different train length. After a parametric study on the 3 basic parameters, variational parametric studies are carried out to understand the effects of the velocity of the train, the gap between the train and the blockage ratio. Through the current numerical study, some conclusions are drawn as follows :

- 1) Through the comparisons with experimental results including the 45 degree slanted entry, the developed solution procedure is proved to be useful to study the 3 dimensional flow physics.
- 2) One-dimensional pressure distribution along the tunnel is valid except the vicinity of the train though the position of the train is eccentric in the tunnel. And this physics remains valid during the crossing event.
- 3) The strength of the side force variation depends mainly on the nose shape of a train, and that of drag force variation depends mainly on the location where the crossing event occurs.
- 4) If the viscous effect is not considered, the side force during the crossing is proportional to the square of the train velocity (V_T). This is valid wherever the location of the crossing event is and whatever the shape of the nose is.
- 5) The effects of the gap change with respect to the reference value are investigated, and practically useful data are obtained. The crossing location does not affect the side force variation($(\Delta C_s)_1$) when the gap is changed.
- 6) If the blockage ratio is increased, namely if the cross sectional area of the tunnel is downsized, the peak values of the side force are shifted due to the suction effect. However, the blockage ratio does not take effects on the change of the side force($(\Delta C_s)_1$).

ACKNOWLEDGEMENT

The authors would like to express sincere appreciation to E. A. Demmenie and W. B. de Wolf at National Aerospace Laboratory NLR in Netherlands for their technical support of experiments in the paper. The authors also appreciate the financial supports from the Government of Korea. This research is a partial result of 'Aerodynamic Design & Analyses of High-Speed Railway System'.

REFERENCES

- (1) Peters, J.L., Aerodynamics of very high speed trains and maglev vehicles: State of the art and future potential, Int. J. of Vehicle Design, Technological Advances in Vehicle Design Series, SP3, Impact of Aerodynamics on Vehicle Design(1983), pp. 308-341.
- (2) Maeda, T. et al, Effect of Shape of Train Nose on Compression Wave Generated by Train Entering Tunnel, Proceedings of the International Conference on Speedup Technology for Railway and Maglev Vehicles, PS3-8(1993), pp. 315-319.
- (3) Roe,P.L., Approximate Riemann Solvers, Parameter Vectors, and Difference Schemes , Journal of Computational Physics, Vol. 43(1981), pp. 357~372.
- (4) Van Albada, G.D., Van Leer, B.D. and Roberts, W.W., A Comparative Study of Computational Methods in Cosmic Gas Dynamics, Astron. Astrophysics, vol. 108(1982), pp. 76-84.
- (5) Hwang, J. and Lee, D, Numerical Simulation of Flow field around High Speed Trains Passing by Each Other, AIAA Paper 99-3156(1999).
- (6) Jameson, A., and Yoon, S., Lower-Upper Implicit Schemes with Multiple Grids for the Euler Equations , AIAA Journal, Vol. 25(1987), pp. 929~935.
- (7) Hyun, B., Numerical Simulation of the Unsteady Flowfield around a Rocket with Canted

- Fins, Ph.D Thesis, Seoul National University(2000)
- (8) Steger,J.L., Dougherty,F.C., Benek,J.A., A Chimera Grid Scheme , Advances in Grid Generation, FED Vol.5, ASME, edited by Ghia,K.N., New York(1983), pp59-69.
- (9) Dougherty, F.C., Development of a Chimera Grid Scheme with Applications to Unsteady Problems, Ph.D Dissertation, Stanford University(1985)
- (10) Mestreau, E., Lohner, R. and Aita, S., TGV Tunnel Entry Simulations Using a Finite Element Code with Automatic Remeshing, AIAA 93-0890(1993)
- (11) T. Ogawa and K. Fujii, Numerical Simulation of Compressible Flows induced by a Train Moving into a Tunnel, Computational Fluid Dynamics Journal, Vol.3 No.1 (1997), p.63-82.
- (12) T. Ogawa and K. Fujii, Numerical Investigation of Three Dimensional Compressible Flows Induced by a Train Moving Into a Tunnel, Computers & Fluids, Vol. 26, No. 6.(1997), pp 565-585.
- (13) Fujii, K. and T. Ogawa, Aerodynamics of High Speed Trains Passing by Each Other Computers & Fluids, Vol. 24, No. 8(1995), pp 897-908.
- (14) Fujii, K., Unified Zonal Method Based on the Fortified Solution Algorithm, ISAS Report No. 648.(1992)
- (15) Holmes,B.S., Dias,J., Rifai,S.M., Buell,J.C.,Johan,Z., Sassa,T., Sato,T., Solution of train-tunnel entry flow using parallel computing , Computational Mechanics 23(1999), pp124-129
- (16) Yoon, T., Lee, S., Hwang, J and Lee, D., Prediction and validation on the sonic boom by a high speed train entering a tunnel, J. of Sound and Vibration,(2000,submitted for publication)
- (17) Kikichi, K., Maeda, T. and Yanagizawa, M., Numerical Simulation of The Phenomena Due to The Passing-by of Two Bodies Using The Unsteady Boundary Element Method, International J. For Numerical Method In Fluids, vol. 23(1996), pp. 445-454
- (18) Shimbo, Y., Hosaka, S., Steady and Unsteady Pressure Measurement on High Speed Train, Proceedings of the International Conference on Speedup Technology for Railway and

Maglev Vehicles, PS3-14(1993), pp341-346.

- (19) Kim, H., Aerodynamic Analysis of a Train Running in a Tunnel(II) Aerodynamics of Two-Trains , Transaction of KSME(in Korean), pp983-995, No.8(1997), pp. 21-36.

LIST OF TABLES

Table. 1 Definition of the cases of crossing

Table. 2 Number of grid points and initial distances used for the crossing cases

Table. 3 Computed cases for the investigation of the effect of the velocity

LIST OF FIGURES

Figure 1. Problem definition about the crossing cases

Figure 2. Schematic diagram for domain decomposition and boundary condition

Figure 3. Shape of Model Train(y-axis : radius, x-axis nose length in mm each)

Figure 4. Grid system for computation of single track case(421,615 for 5 blocks)

Figure 5. Pressure contour representing the generation and the propagation of the compression wave at a speed of 350km/h and with non-slanted entry (nondimensional time = 60 sec)

Figure 6. Comparison with measured at 4.3% from the entry of the tunnel and predicted entry compression wave with non-slanted entry for 300km/h

Figure 7. Effect of the 45 degree slanted entry on incident compression wave at 4.3% from the entry of the tunnel at a speed of 350km/h

Figure 8. Frontal view of grid system for crossing case and location of tunnel wall pressure probes

Figure 9. Tunnel wall pressure distributions at nondimensional time = 30,40,50,60 for the case SFCT

Figure 10. Tunnel wall pressure distributions at nondimensional time = 110,120,130,140 for the case SFCT

Figure 11. Tunnel wall pressure distributions at nondimensional time = 30,36,42,48 for the case LFCT

Figure 12. Tunnel wall pressure distributions at nondimensional time = 78,84,90,96 for the case LFCT

Figure 13. Aerodynamic load history for a)the case SFCO(2 cars) and b)the case SFCO3(3 cars)

Figure 14 Comparison of aerodynamic force coefficients for 2 car cases : a) Side force coefficient, b) Drag coefficient

Figure 15. Side force histories for fore,mid and aft car for the case SFCO3 in physical values at a speed of 350km/h during the crossing.

Figure 16. Extension of side force history to a multi-car train

Figure 17. Top view of pressure field of the crossing event in the tunnel(LFCT)

Figure 18. Top view of pressure field of the crossing event at the open space(LFCO)

Figure 19. C_s histories with velocity changes for the case a) LFCO, b) SFCO , c) LFCT

Figure 20. C_s histories with gap changes for the case a) LFCO, b) LFCT

Figure 21. Definition of output parameters for the crossing problems

Figure 22. Comparison of the defined output parameter along gap changes between the case LFCT and LFCO

Figure 23. Effect of blockage ratio change for the case LFCT a) C_s histories b) A view of change of the defined output parameter along blockage ratio changes

APPENDIX : NOMENCLATURE

a_∞	speed of sound
C_s	side force coefficient
C_D	drag force coefficient
C_L	lift force coefficient
D	width of tunnel or height of tunnel
e	total energy per unit volume

E, F, G	inviscid flux vector
FDS	Flux Difference Splitting
FSA	Fortified Solution Algorithm
GLS	Galerkin Least Squares
MUSCL	Monotone Upstream-Centered Scheme for Conservation
p'	acoustic pressure
P	pressure
L	length of tunnel
Q	vector of conservative variables
r	distance between a source position at the sound generation time and an observer at the sound receiving time
x, y, z	cartesian coordinates
u, v, w	velocity components in x, y, z direction
V_T	velocity of train
t	observer time
γ	ratio of specific heat
ρ	density
\vec{n}	normal vector on the surface
θ	angle between the normal vector on the surface and the radiation vector
τ	retarded time
Δt	computational time step

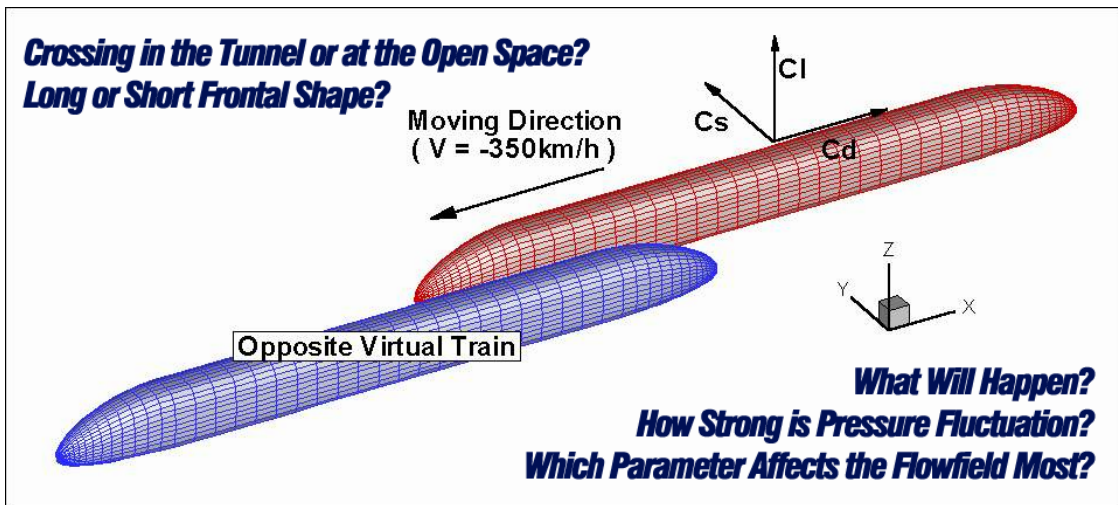


Figure 1. Problem definition about the crossing cases

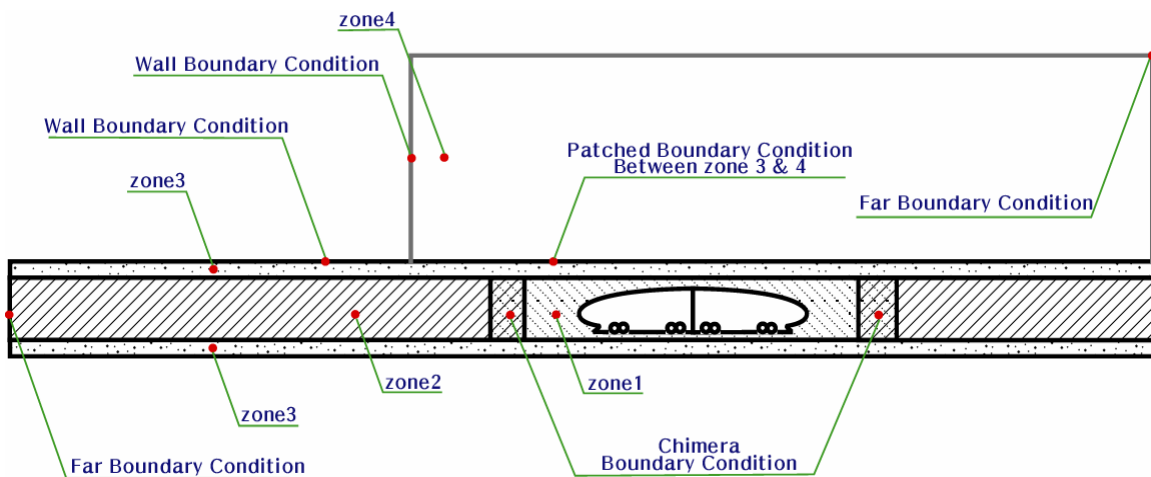


Figure 2. Schematic diagram for domain decomposition and boundary condition

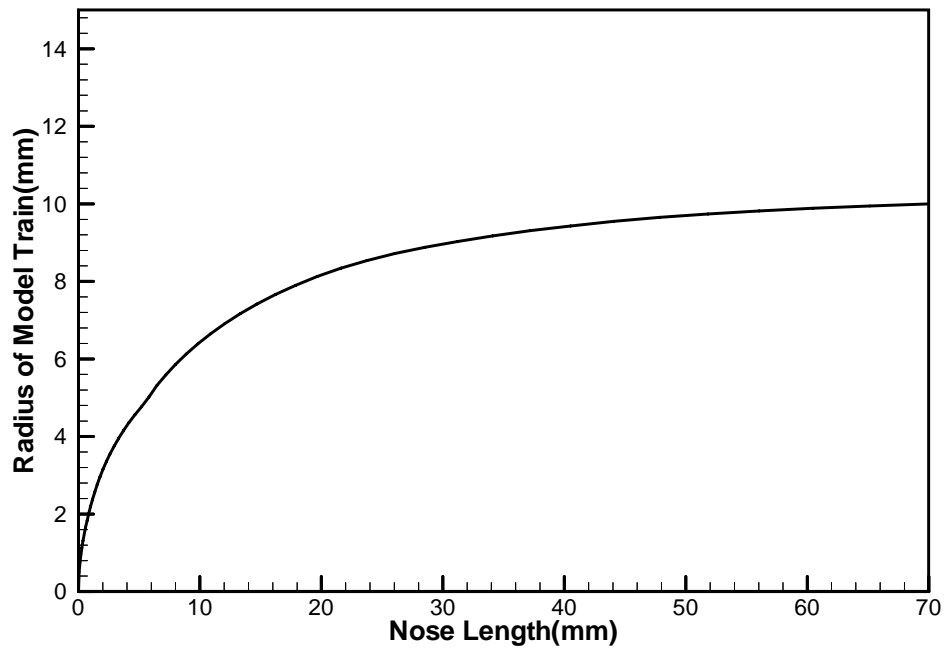


Figure 3. Shape of Model Train(y-axis : radius, x-axis nose length in mm each)

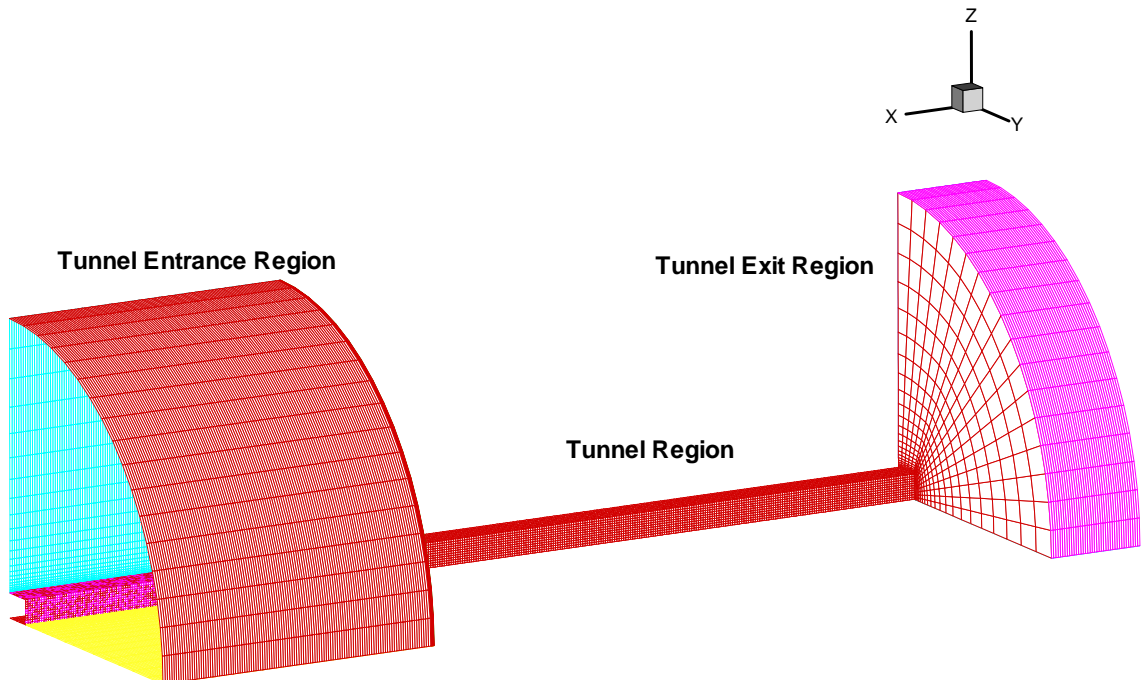


Figure 4. Grid system for computation of single track case(421,615 for 5 blocks)

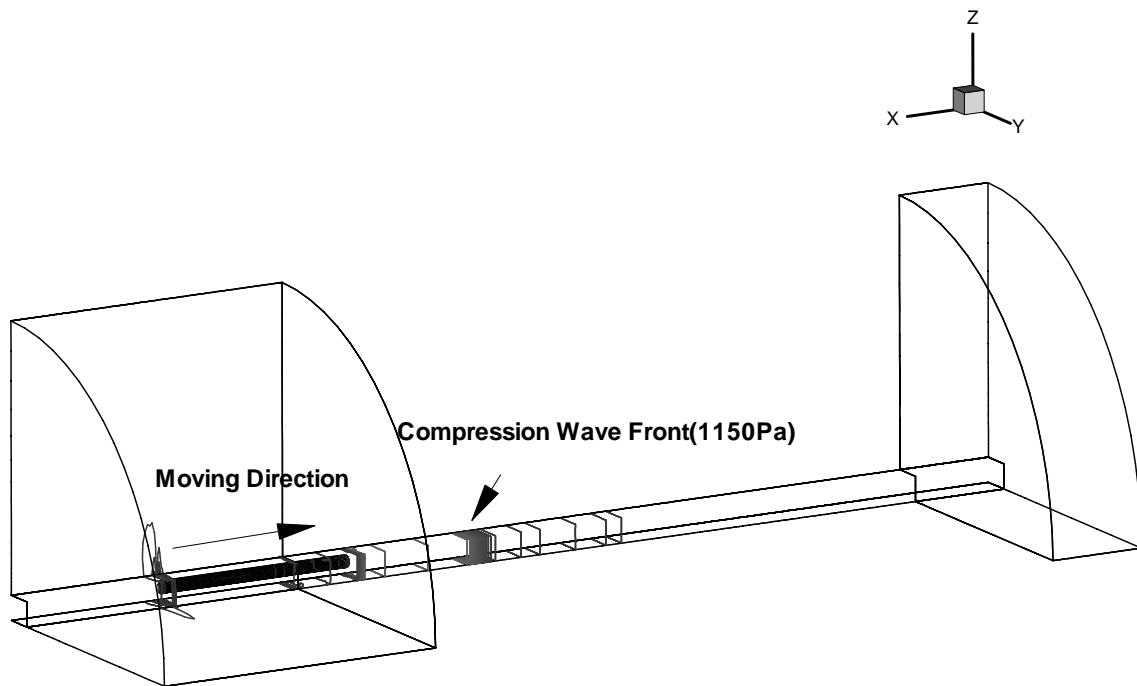


Figure 5. Pressure contour representing the generation and the propagation of the compression wave at a speed of 350km/h and with non-slanted entry (nondimensional time $V_T t/D = 60$)

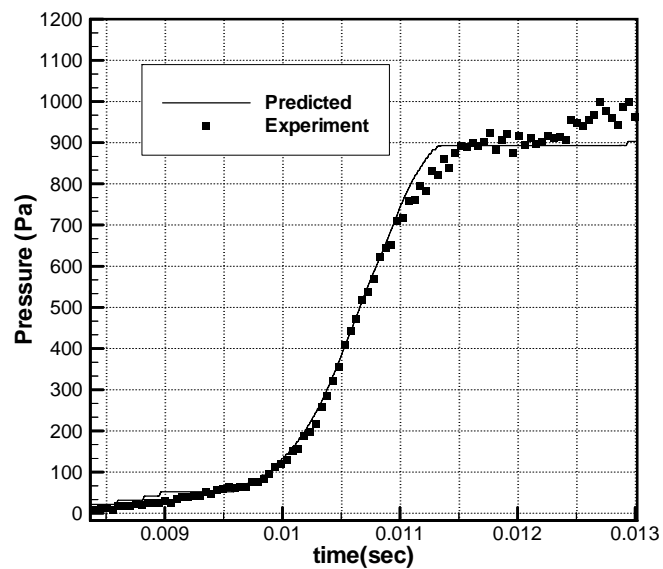


Figure 6. Comparison with measured at 4.3% from the entry of the tunnel and predicted entry compression wave with non-slanted entry for 300km/h

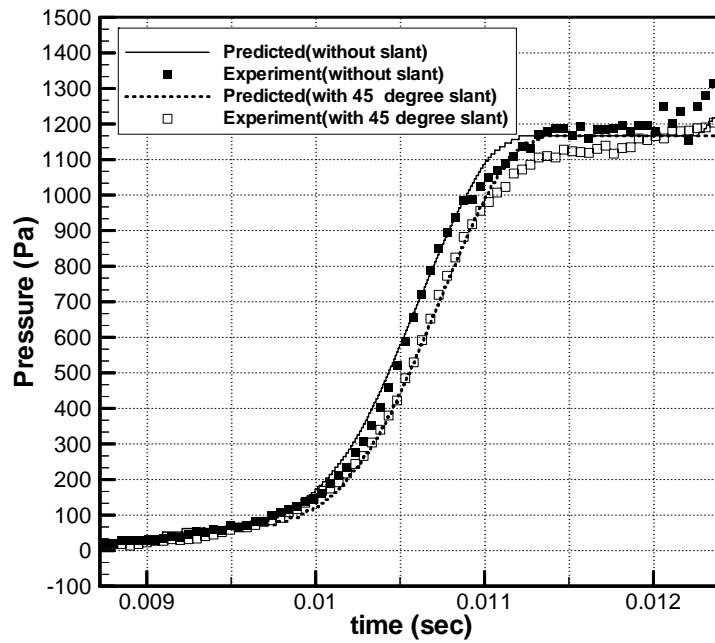


Figure 7. Effect of the 45 degree slanted entry on incident compression wave at 4.3% from the entry of the tunnel at a speed of 350km/h

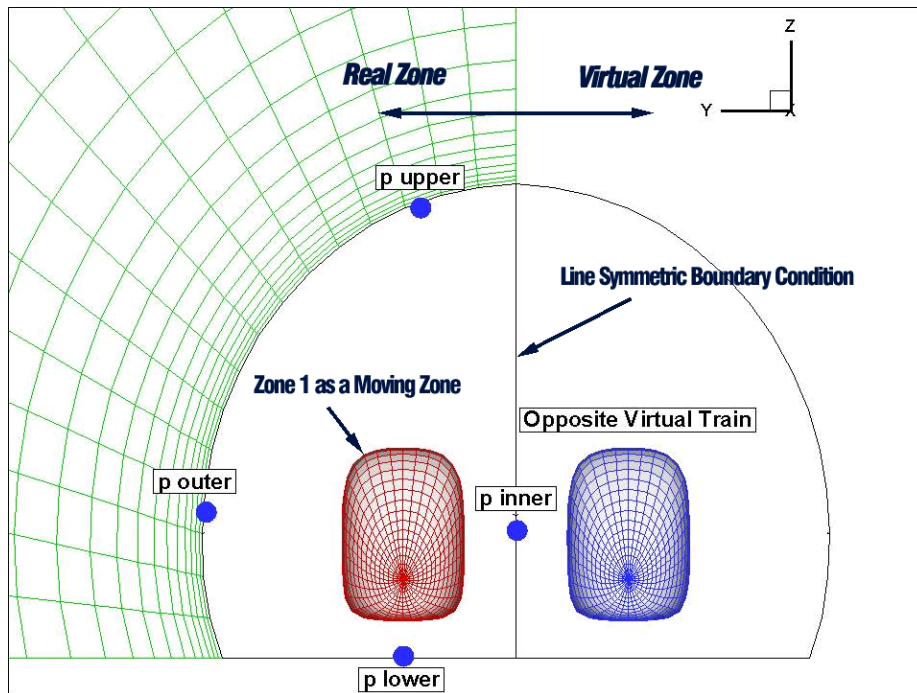


Figure 8. Frontal view of grid system for crossing case and location of tunnel wall pressure probes

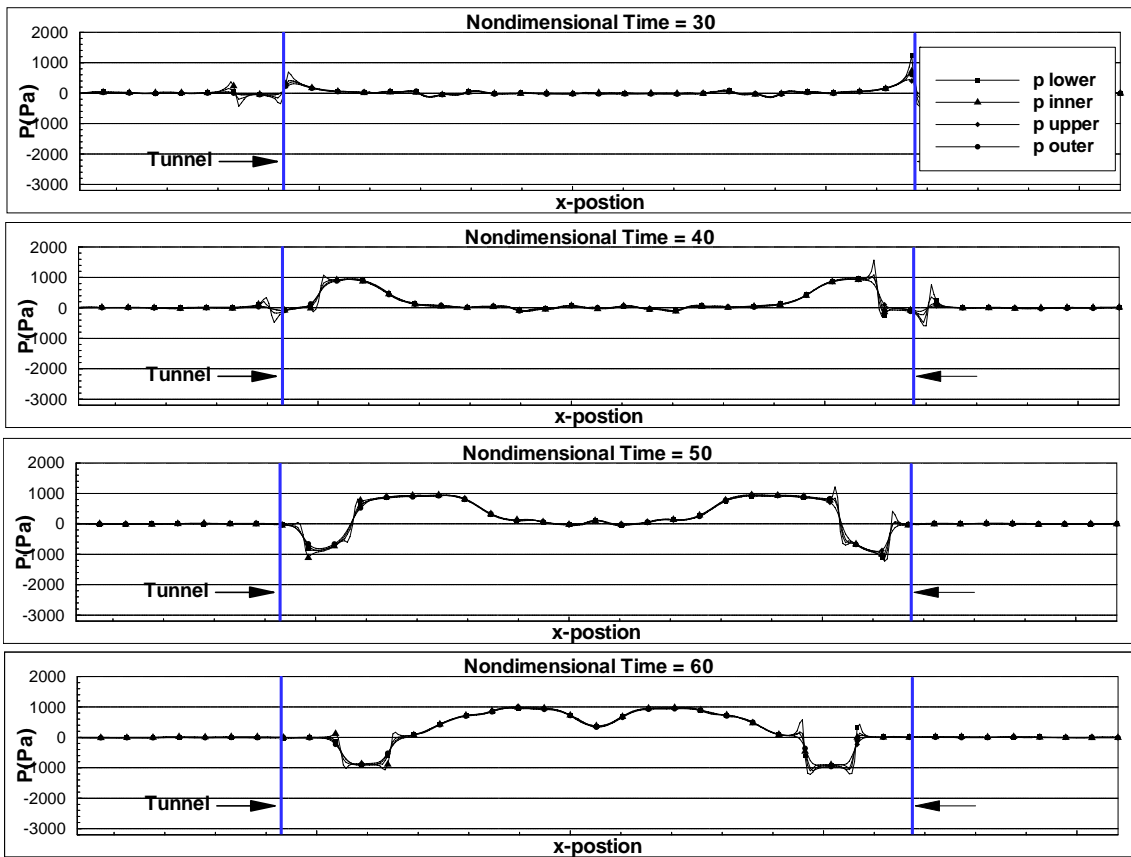


Figure 9. Tunnel wall pressure distributions at nondimensional time = 30,40,50,60 for the case SFCT

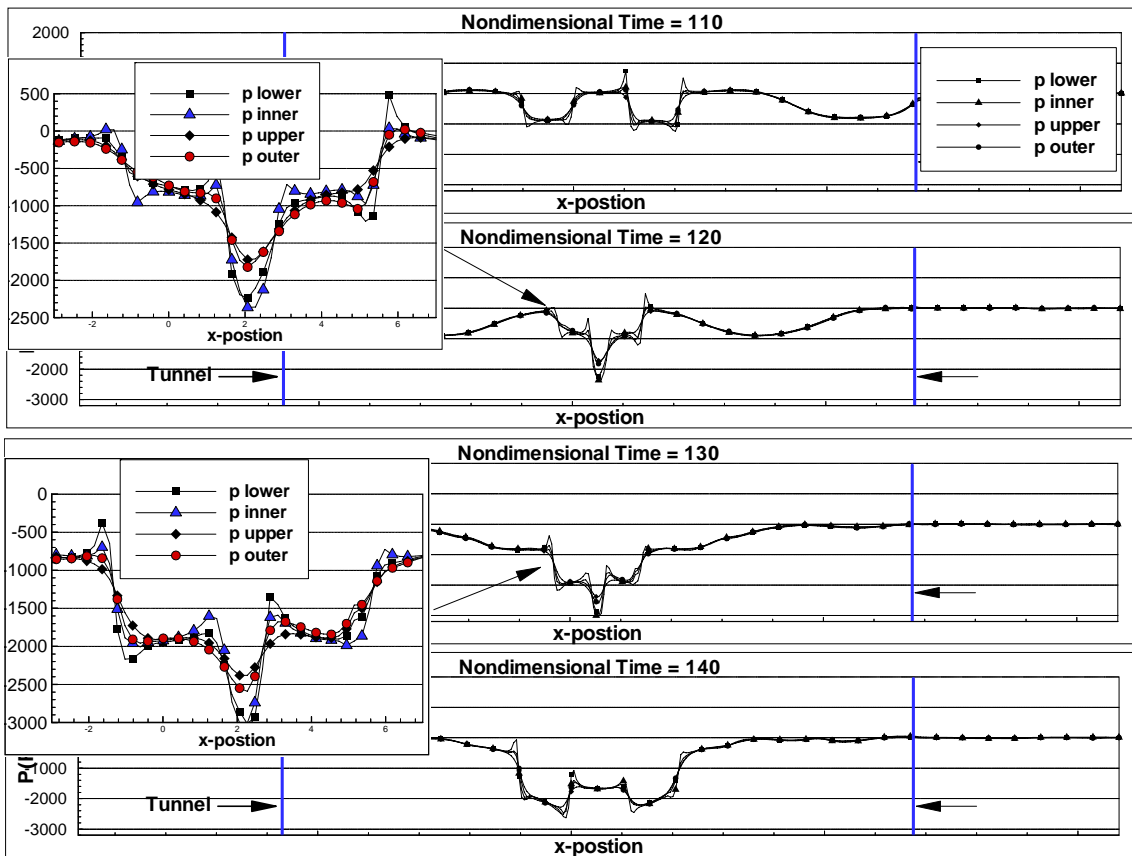


Figure 10. Tunnel wall pressure distributions at nondimensional time = 110,120,130,140 for the case SFCT

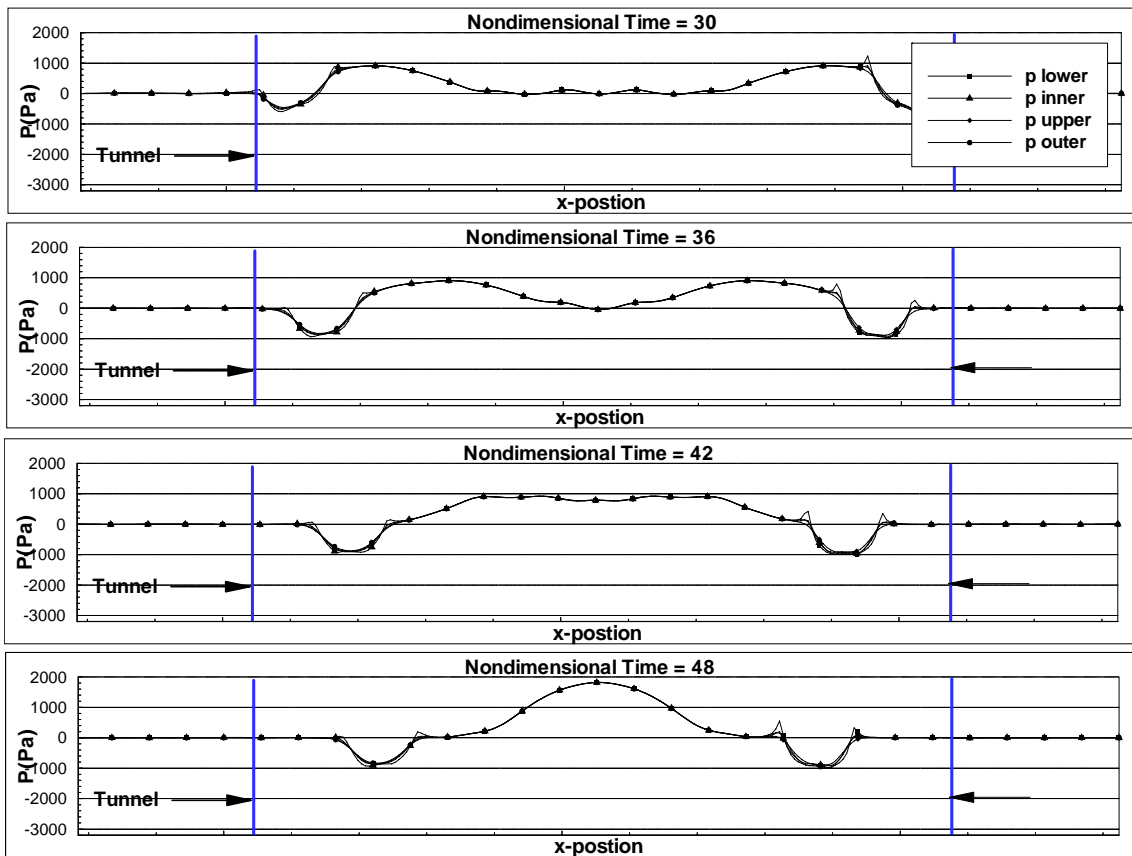


Figure 11. Tunnel wall pressure distributions at nondimensional time = 30,36,42,48 for the case LFCT

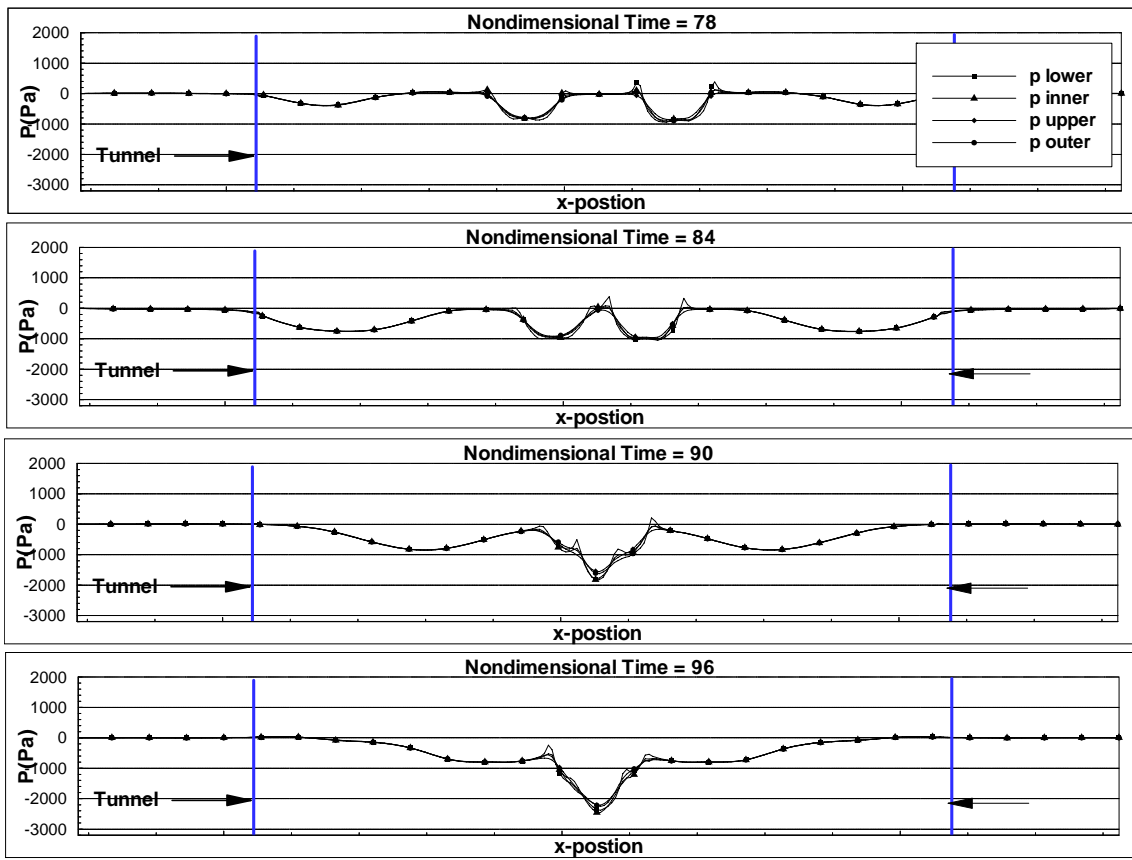
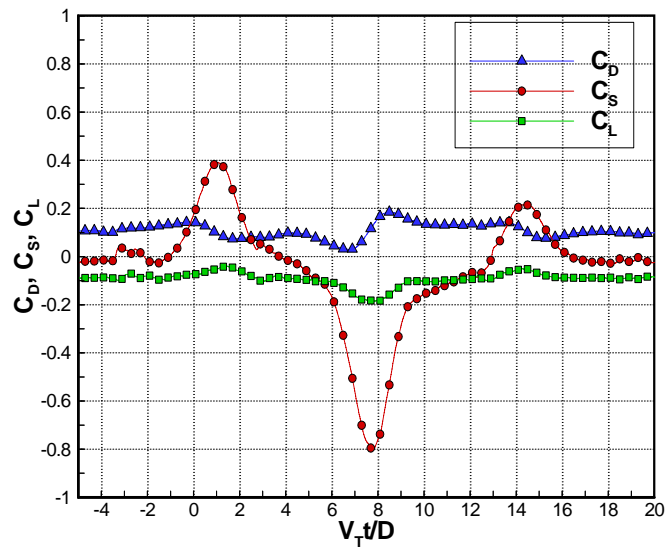
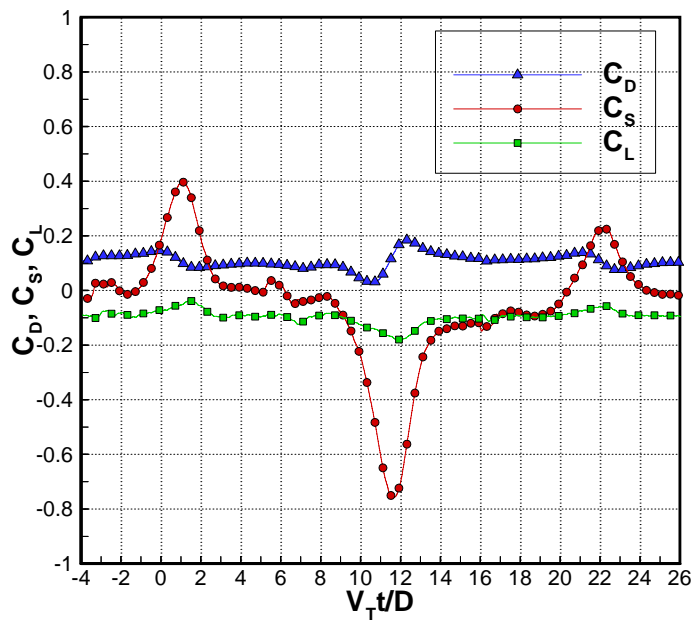


Figure 12. Tunnel wall pressure distributions at nondimensional time = 78,84,90,96 for the case LFCT

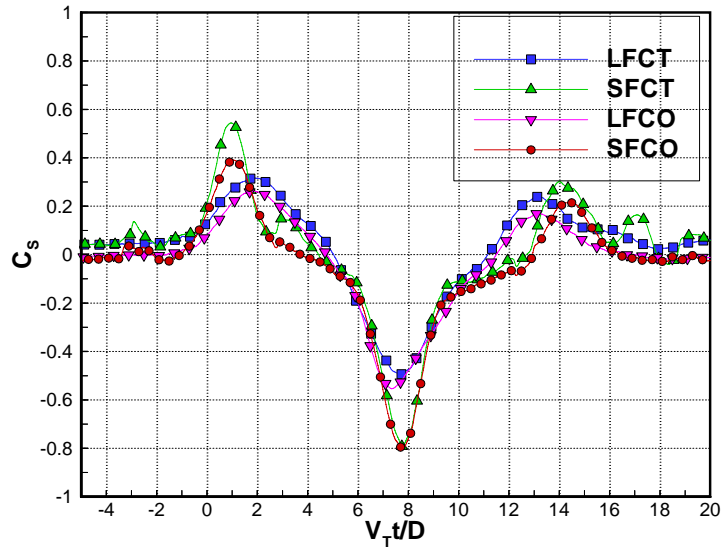


a)

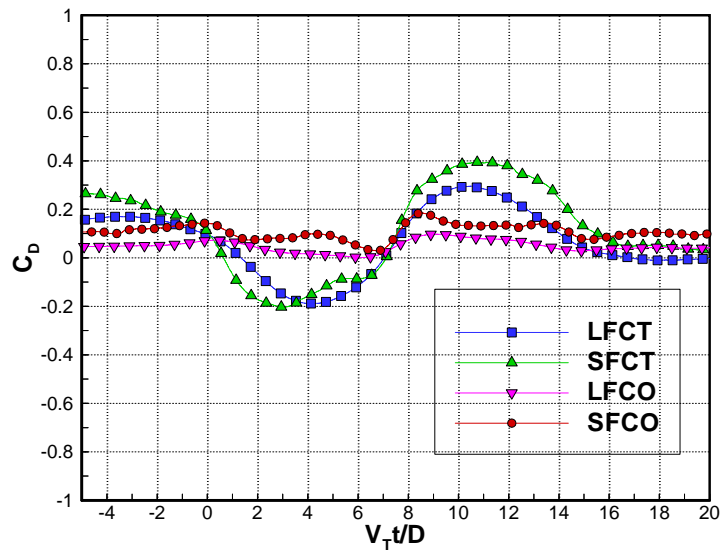


b)

Figure 13. Aerodynamic load history for a) the case SFCO(2 cars) and b) the case SFCO3(3 cars)



a)



b)

Figure 14 Comparison of aerodynamic force coefficients for 2 car cases : a) Side force coefficient, b) Drag coefficient

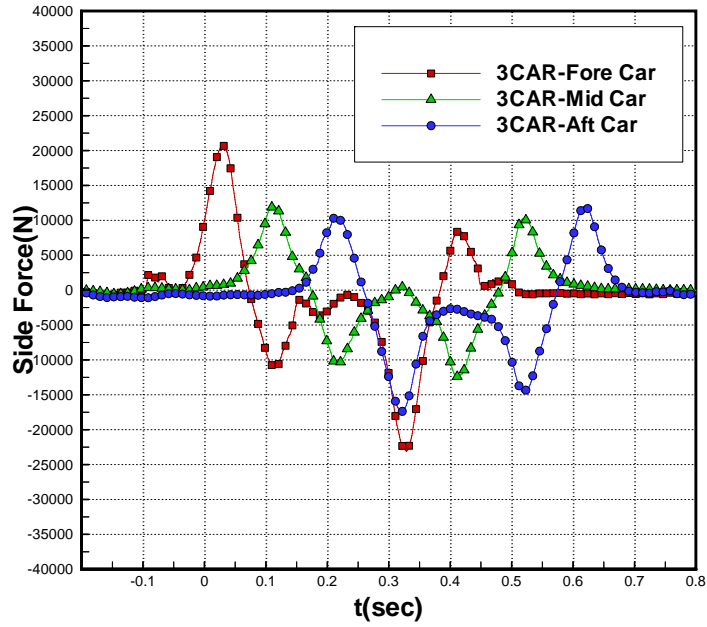


Figure 15. Side force histories for fore, mid and aft car for the case SFCO3 in physical values at a speed of 350km/h during the crossing.

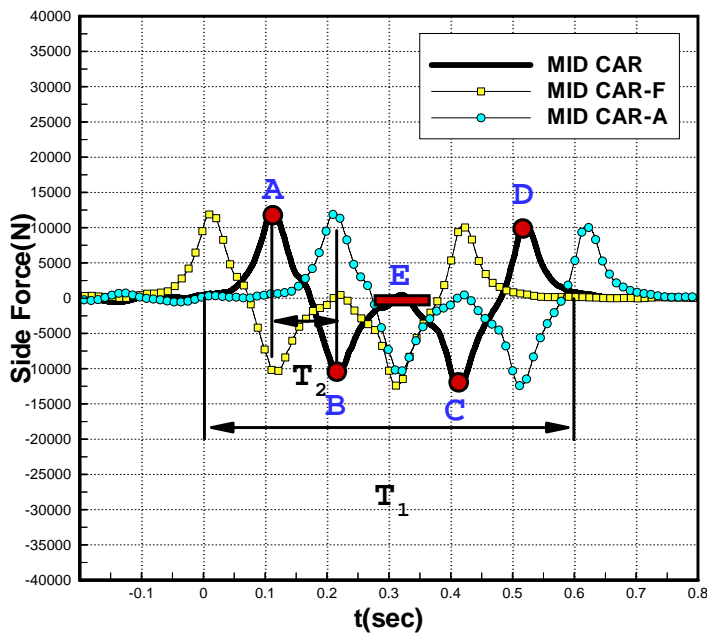


Figure 16. Extension of side force history to a multi-car train

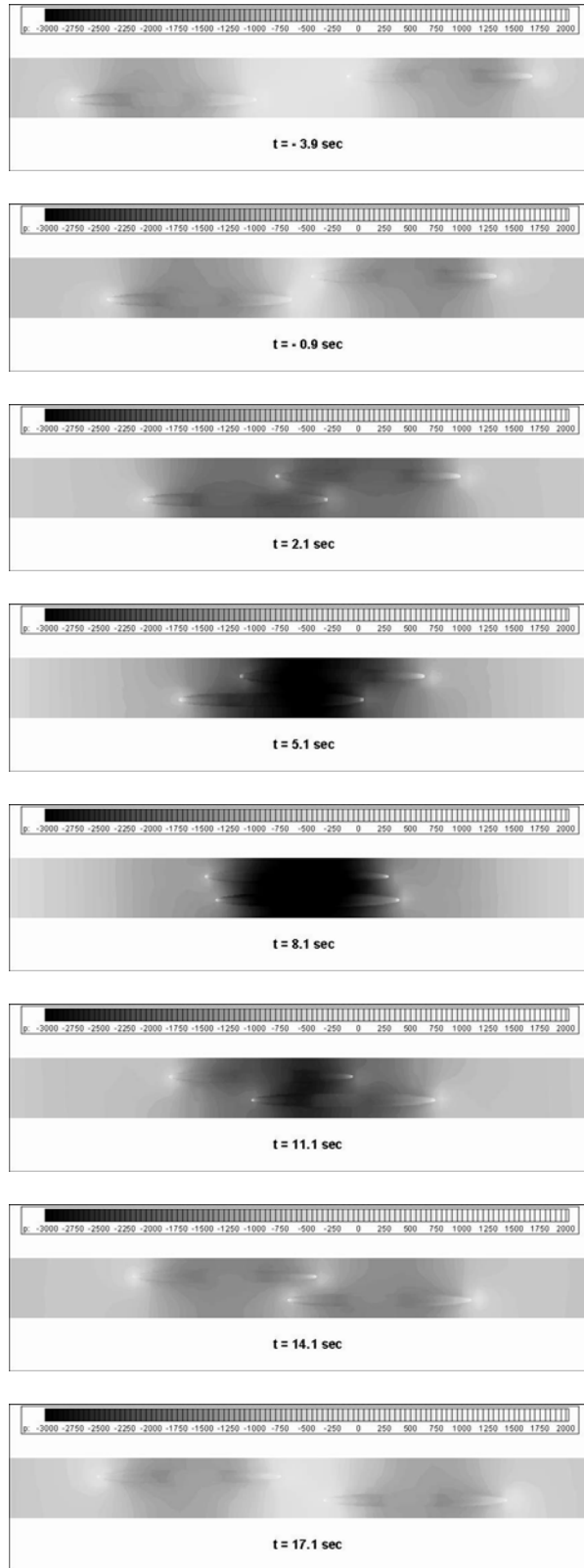


Figure 17. Top view of pressure field of the crossing event in the tunnel(LFCT)

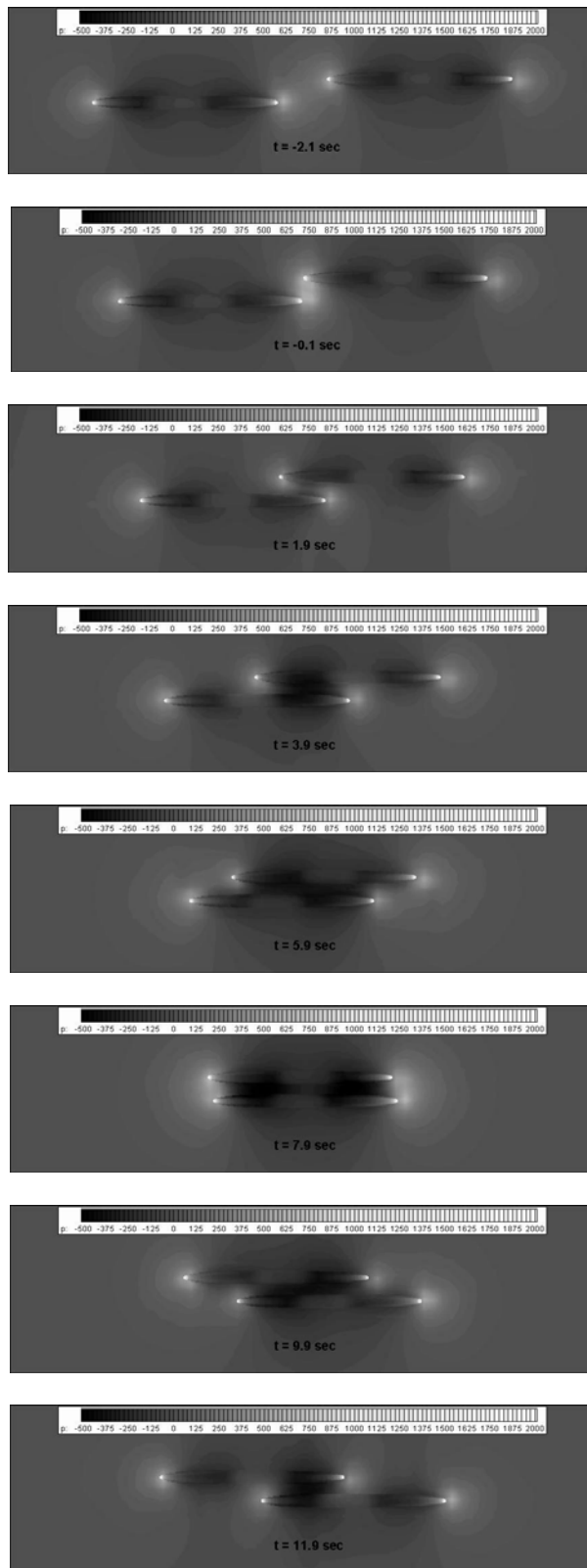
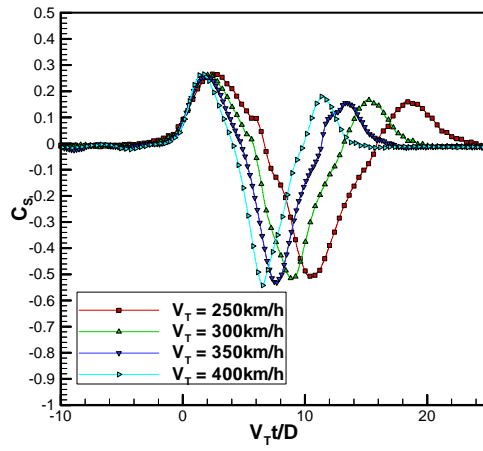
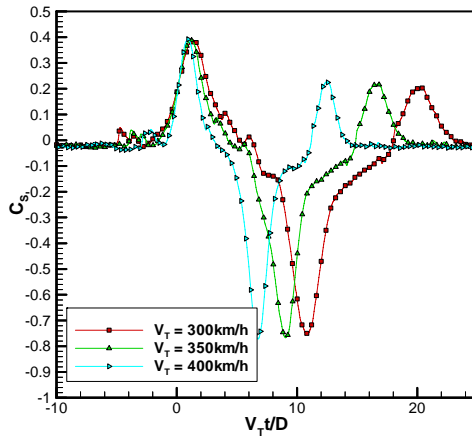


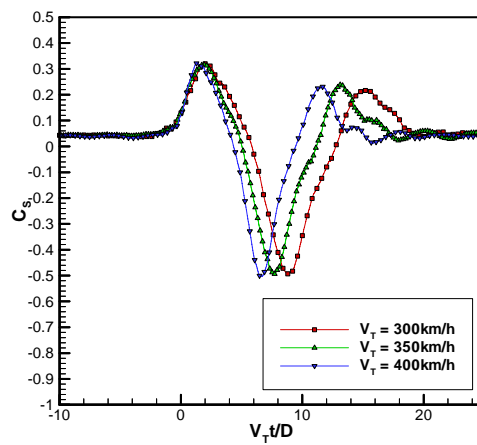
Figure 18. Top view of pressure field of the crossing event at the open space(LFCO)



a)

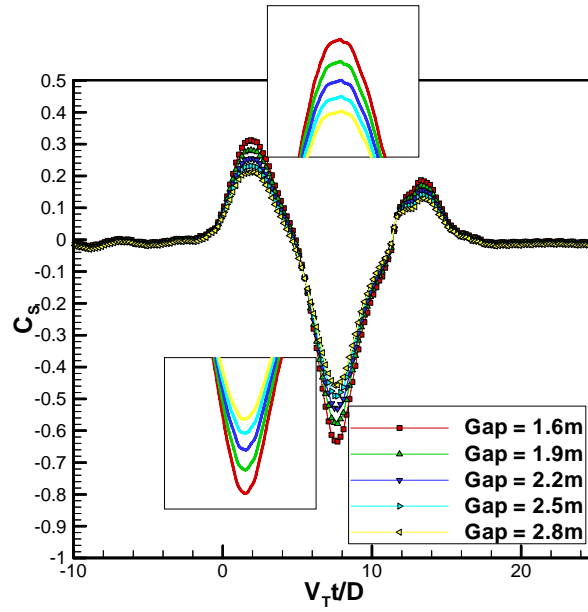


b)

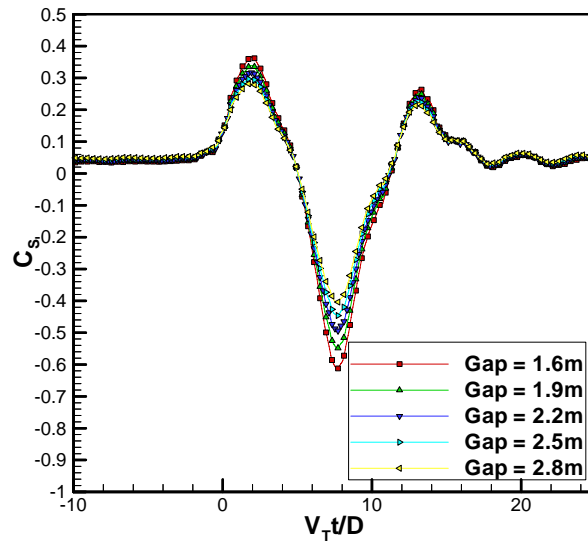


c)

Figure 19. C_s histories with velocity changes for the case a) LFCO, b) SFCO, c) LFCT



a)



b)

Figure 20. C_s histories with gap changes for the case a) LFCO, b) LFCT

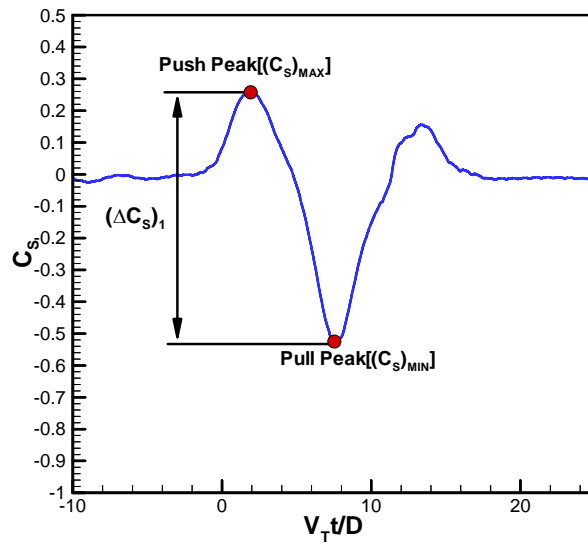


Figure 21. Definition of output parameters for the crossing problems

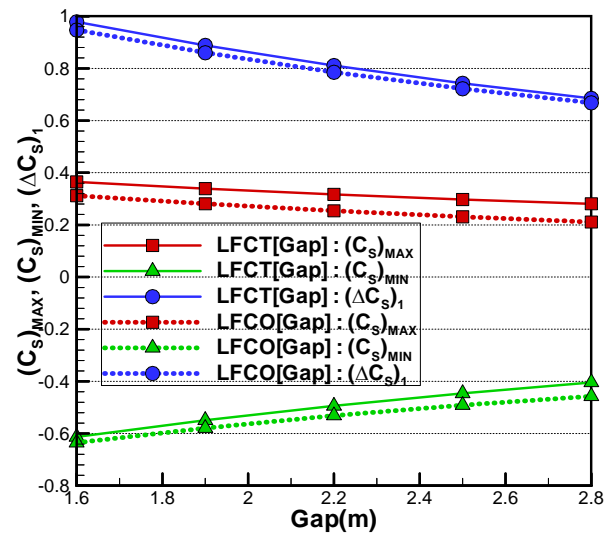
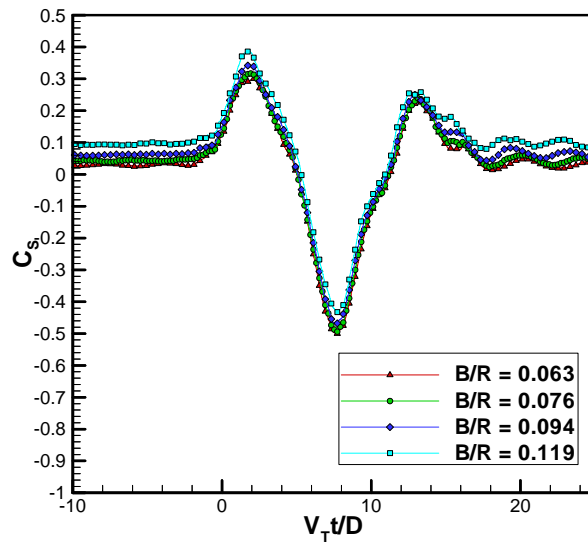
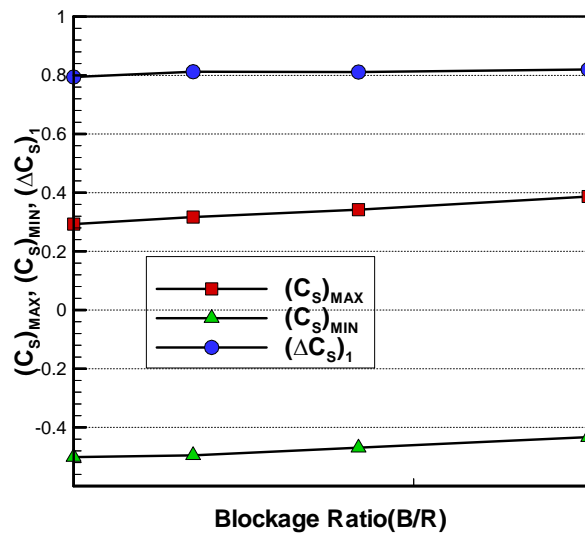


Figure 22. Comparison of the defined output parameter along gap changes between the case LFCT and LFCO



a)



b)

Figure 23. Effect of blockage ratio change for the case LFCT a) C_s histories b) A view of change of the defined output parameter along blockage ratio changes